HHS Public Access

Author manuscript

J Immunol. Author manuscript; available in PMC 2016 April 15.

Published in final edited form as:

J Immunol. 2015 April 15; 194(8): 3984–3996. doi:10.4049/jimmunol.1402897.

HkRP3 is a Microtubule-Binding Protein Regulating Lytic Granule Clustering and NK Cell Killing

Hyoungjun Ham[*,†], **Walter Huynh**[‡], **Renee A. Schoon**[†,§], **Ronald D. Vale**[‡], and **Daniel D. Billadeau**[†,§]

[*]Mayo Graduate School, University of California, San Francisco, CA 94158

[†]Department of Immunology, University of California, San Francisco, CA 94158

[‡]Department of Cellular and Molecular Pharmacology and the Howard Hughes Medical Institute, University of California, San Francisco, CA 94158

[§]Division of Oncology Research and Schulze Center for Novel Therapeutics, College of Medicine, Mayo Clinic, 200 First Street SW, Rochester, MN 55905

Abstract

NK cells provide host defense by killing viral-infected and cancerous cells through the secretion of preformed lytic granules. Polarization of the lytic granules toward the target cell is dependent on an intact microtubule (MT) network as well as MT motors. We have recently shown that DOCK8, a gene mutated in a primary immunodeficiency syndrome, is involved in NK cell killing in part through its effects on MTOC polarization. In this study, we identified Hook-related protein 3 (HkRP3) as a novel DOCK8- and MT-binding protein. We further show that HkRP3 is present in lytic granule fractions, interacts with the dynein motor complex and MTs. Significantly, depletion of HkPR3 impaired NK cell cytotoxicity, which could be attributed to a defect in not only MTOC polarity, but also impaired clustering of lytic granules around the MTOC. Our results demonstrate an important role for HkRP3 in regulating the clustering of lytic granules and MTOC repositioning during the development of NK cell-mediated killing.

INTRODUCTION

Natural killer (NK) cells are lymphocytes of the innate immune system that play an essential role in the clearance of viral-infected cells and cancer cells (1, 2). Various germline-encoded activating and inhibitory receptors are expressed on the surface of NK cells, and current knowledge suggests that integrated signals from these receptors enable NK cells to distinguish unhealthy ‘non-self’ cells from healthy ‘self’ cells, thereby regulating NK cell activation (3). The main consequence of NK cell activation is the killing of bound target cells via the directed secretion of preformed secretory lysosomes called lytic granules.

Correspondence: Daniel D. Billadeau, Division of Oncology Research and Schulze Center for Novel Therapeutics, College of Medicine, Mayo Clinic, 200 First Street SW, Rochester, MN, 55905, USA; billadeau.daniel@mayo.edu; Phone: (507) 266-4334; Fax: (507) 266-5146.

Multiple molecular features are observed during NK cell-mediated cytotoxicity. For example, after the initial adhesion to target cells, NK activating receptors as well as integrins and F-actin, accumulate at the center of the NK-target interface, forming the cytotoxic synapse (CS)(3-5). Concurrent with this, lytic granules are rapidly clustered around the microtubule-organizing center (MTOC) by the dynein-dynactin minus-end-directed microtubule (MT) motor complex that constitutively associates with lytic granules (6). Subsequently, the MTOC is polarized toward the CS to allow directed secretion of the lytic granule contents toward the bound target cell. Therefore, delivery of lytic granules is dependent upon tight regulation of both the MT network as well as its associated motor proteins. However, the detailed mechanism for this regulation remains elusive.

Dedicator of cytokinesis 8 (DOCK8) deficiency is a primary immunodeficiency that affects NK cell cytotoxicity (3, 7, 8). This disease is inherited in an autosomal recessive pattern, and the main clinical symptoms are elevated serum IgE levels, recurrent infections in the lung and skin, and severe allergies (9-11). Others and we have previously shown that DOCK8 is a CDC42 guanine nucleotide exchange factor and DOCK8-deficient/-depleted human NK cells show defective cytotoxic activity (7, 8, 12). At the molecular level, DOCK8 deficiency resulted in defective accumulation of F-actin at the CS, impaired integrin-mediated adhesion, and MTOC polarization (7, 8, 13). Using mass spectrometry (MS), we previously found that DOCK8 interacted with WASP and talin, two key regulators of F-actin generation and integrin affinity maturation, respectively (8). Significantly, depletion of DOCK8 led to a reduced recruitment of both proteins to the CS, which may account in part for the defects in F-actin accumulation and integrin-mediated adhesion. Mechanisms by which DOCK8 contributes to MTOC polarization are not known.

In the present study, we characterize a protein known as Hook-related protein 3 (HkRP3, also called CCDC88B, FLJ00354, or Gipie) as a novel DOCK8-interacting protein. HkRP3 is one of three members of the Girdin protein family, which include Girdin and Daple (14, 15). All Girdin family members contain an N-terminal region with sequence homology to the microtubule-binding domain of Hook proteins. In addition, all members contain a long coiled-coil region at their center and a variable unique region at the C-terminus. Previously, Matsushita and colleagues reported that HkRP3 is an important regulator of endoplasmic reticulum (ER) stress response in endothelial cells via its interaction with GRP78 (78kDa glucose-regulated protein) (15). However, little is known about cellular roles of HkRP3 in hematopoietic cells, where HkRP3 has been suggested to be preferentially expressed based on expressed sequence tag databases (14, 15). Herein we demonstrate that HkRP3 mediates NK cell cytotoxicity in part through its ability to regulate lytic granule clustering and MTOC polarization. We further show that HkRP3 directly binds to MTs via its unique region at the C-terminus and also interacts with the dynein-dynactin motor complex which transports lytic granules along MTs. Taken together, our results provide a novel cellular function of HkRP3 during the development of NK cell cytotoxicity.

MATERIALS AND METHODS

Cells, Reagents, and Antibodies

YTS cells were obtained from Dr. E. Long (NIH, Bethesda, MD) and NKL cells from Dr. M. Robertson (Indiana University Cancer Center, Indianapolis, IN), and primary human NK cells were cloned and passaged as previously described (16). Two separate rabbit polyclonal antisera to HkRP3 (NCBI: NP_115627.6) were obtained by immunizing rabbits with glutathione S-transferase (GST)-conjugated HkRP3 amino acids 821-927 (anti-HkRP3 (1)) and amino acids 1387-1476 (anti-HkRP3 (2)) (Cocalico Biologicals Inc., Reamstown, PA). Anti-HkRP3 (1) was used for immunoblot and immunoprecipitation and anti-HkRP3 (2) was used for immunofluorescence assays in this study. Polyclonal rabbit anti-serum for DOCK8 was previously described (8). Antibodies for α-tubulin, γ-tubulin, and FLAG (clone M2) were purchased from Sigma Aldrich, and antibodies for MBP (Immunology Consultants Lab, Inc.), $p150^{Glued}$ (BD), dynein intermediate chain (Millipore), β-actin (Cell Signaling), and granzyme B (Santa Cruz) were purchased as indicated. Nocodazole was purchased from Selleckchem.com.

Small Interfering RNA (siRNA) Constructs and Nucleofection

siRNA duplexes were obtained from Dharmacon: “siControl: 5’-UUCUCCGAACGUGUCACGU-3’”, “siHkRP3 #1: 5’-GCAUGAGAAUAAAGCUGAA-3’”, “siHkRP3 #2: 5’-GGCAGGAGUUGGCAAGAGA-3’”, and “siDOCK8: 5’-GGAGAUUAUUUGUGAACUU-3’”. Nucleofection of siRNA oligos into YTS, NKL and NK clones was performed as previously described (17, 18).

Plasmids and Transfection

The pCI2.FLAG.YFP.DOCK8 construct was previously described (8). Full-length HkRP3 (NCBI: NP_115627.6) was cloned into the pCI2 plasmid in-frame with FLAG.YFP or EE. All constructs were sequenced validated in the Gene Analysis Core shared resource of the Mayo Clinic Comprehensive Cancer Center. HEK293T cells were transfected using polyethylenimine (PEI, Polysciences). HEK293T cells were prepared in 10 cm cell-culture plates at 70-80% confluency on the day of transfection. 6 μg of total plasmid DNA was diluted in 400 μl of OptiMEM media (Gibco), and 72 μl of PEI dissolved in water (2 mg/ml) were added. After 15 minutes of incubation at room temperature, the volume of medium in the cell-culture plate was adjusted to 5 ml, and the mixture was added to HEK293T cells drop-wise. Cells with PEI mixture were incubated at 37 °C for 90 min, and the media was then changed with fresh growth medium. Experiments were performed 48 hours after transfection.

Immunoprecipitation and GST pull-down assays

For immunoprecipitation, cells were lysed in Nonidet P-40 lysis buffer (25 mM HEPES [pH 7.9], 25 mM NaCl, 0.5% Nonidet P-40, 1 mM EDTA, 0.5 mM $CaCl_2$, 1 mM PMSF, 10 μg/ml leupeptin, and 5 μg/ml aprotinin), and immunoprecipitations were performed as previously described (19). GST fusion protein pull-downs were performed as previously

described (8). To examine direct interactions, 30 μg of GST fusion protein bound to glutathione-agarose slurry was incubated with 30 μg of MBP fusion protein for 3 h at 4 °C.

Microtubule Co-pelleting Assay

Both *in vitro* microtubule assembly and microtubule co-pelleting assays were performed according to the manufacturer's instruction (Cytoskeleton Inc.). Fusion proteins were spun at 120,000 × g for 40 min at 4 °C, and the supernatant was collected before the assay. Various concentrations of microtubules were incubated with 0.5 μM of fusion proteins at room temperature for 30 minutes. Then, samples were spun at 100,000 × g for 40 min at room temperature, and supernatants and pellets were collected for SDS/PAGE analysis. Depending on the molecular weight of fusion proteins used, tubulin and fusion proteins were visualized either by coomassie blue staining or by immunoblotting.

Cytotoxicity Assay

The ^{51}Cr-release assays were performed as previously described (16). All Lytic Unit values in this study were obtained by calculating the required number of NK cells to kill 20% of target cells.

Conjugate Assay

YTS cells were labeled for 30 min at 37 °C with 2.5 μM CellTracker Violet BMQC (Invitrogen), and 721.221 target cells were labeled for 30 min at 37 °C with 0.75 μM CFSE (eBioscience). Labeled cells were then washed and resuspended at 1.6×10^6 cells/ml. Cells (250 μl of each) were mixed together, centrifuged at 200 rpm for 5 min, and allowed to incubate at 37 °C for up to 15 min before fixation by adding 4% paraformaldehyde in PBS. Conjugate formation was assessed using two-color flow-cytometry, and analyzed as the percentage of target-bound NK cells (violet$^+$green$^+$) over total NK cells (violet$^+$).

Microscopy

For microscopy of single siRNA transfected YTS cells, 1.6×10^5 cells were plated on poly-L-lysine (PLL)–coated coverslips for 10 min at 37 °C. For microscopy of conjugated YTS cells with target cells, 250 μl (1.6×10^6 cells/ml in serum-free RPMI 1640 medium) of untransfected or siRNA transfected YTS cells (72 h post transfection) cells were mixed with an equal volume of 7-amino-4-chloromethylcoumarin (CMAC; Invitrogen)–stained 721.221 target cells (1.6×10^6 cells/ml in serum-free RPMI 1640 medium) and centrifuged together at 200 rpm for 5 min. In the case of time-course experiments, cells were incubated at 37 °C for 1, 5, 15, and 25 min, resuspended, and incubated on PLL-coated coverslips for 5 min at 37 °C. In the case of single time-point experiments, the lightly-pelleted cells were incubated at 37 °C for 15 min, resuspended, and allowed to adhere to PLL–coated coverslips for 10 min at 37 °C. For stimulation of YTS cells with antibody-coated coverslips, antibody-coated coverslips were prepared as previously described using anti-CD28 antibody (BD) and anti-CD45 antibody (BD) (17). YTS cells were then dropped on coverslips and incubated for 25 min at 37 °C.

Cells were fixed with either methanol or 4% paraformaldehyde in PBS and stained with specific Abs (anti-HkRP3, anti–LFA-1 [clone MHM23], anti-perforin [BD Biosciences],

anti-α-tubulin [Sigma Aldrich], anti-γ-tubulin [Sigma Aldrich], anti-p150^{Glued} [BD], and anti-dynein intermediate chain [Millipore]). Secondary reagents included FITC-, tetramethylrhodamine-, Alexa Fluor 568-, or Alexa Fluor 488–labeled goat anti-mouse IgG, or goat anti-rabbit IgG (Invitrogen). F-actin was visualized with Alexa488-phalloidin or rhodamine-phalloidin (Invitrogen). Coverslips were mounted on glass slides using SlowFade reagent (Invitrogen) and examined on microscopes at room temperature. Most of the prepared slides were examined with a Plan-Apochromat 100x/1.46 NA oil immersion objective equipped on an LSM-710 laser-scanning confocal microscope (Carl Zeiss). Additional slides were examined with a Plan-Apochromat 100x/1.40 NA oil immersion objective on an Axiovert 200 microscope (Carl Zeiss) equipped with a digital camera (AxioCam HRC; Carl Zeiss). Images were captured with either the AxioVision or LSM software packages (Carl Zeiss).

Image Analysis

ImageJ software (version 1.45s; NIH) was used for processing of microscopic images in this study. To calculate the mean fluorescence intensity (MFI) of HkRP3 within a cell, whole cell areas enclosed by cortical actin (visualized with fluorescently labeled phalloidin) and the sum intensity of HkRP3 within the region was measured. Quantification of fluorescence intensity for LFA-1 at the YTS-721.221 interface was performed as previously described (8). Images containing a total of 30 conjugates were taken for each condition (10 conjugates per experiment; 3 independent experiments) and analyzed. For quantification of mean distance of lytic granules to the MTOC and distance between the MTOC and the CS, each image was taken after setting the focal plane to visualize γ-tubulin (representing MTOC) of an YTS cell. To calculate the mean distance of lytic granules from the MTOC, we first obtained x and y coordinates of each lytic granule (visualized by perforin stain) in an YTS cell as well as those of γ-tubulin. Then, we weighted each granule to MTOC distance by the granule area before calculating the mean MTOC distance; this method allowed for quantification of clustered lytic granules, which could appear as a single granule in many cases and potentially bias the mean granule to MTOC distance as previously described (6). The assumption for this area-weighted mean distance is that sizes of lytic granules in a specific YTS cell are the same, so the minimum granule area detected in an YTS cell represents a single lytic granule. Taking this assumption, the mean distance between lytic granules to MTOC was calculated using equation (1):

Total granule area $(TGA) = \sum_{i=1}^{n} A_i$ (A_i : area of an individual lytic granule, n : total number of lytic granules)

$$\text{Average distance of lytic granules from MTOC} = \sum_{i=1}^{n} \frac{A_i}{TGA} \times \sqrt{(x - x_i)^2 + (y - y_i)^2} \quad (1)$$

where x and y represent coordinates of the MTOC centroid, x_i and y_i are coordinates of an individual lytic granule centroid, A_i is the area of an individual lytic granule, and n represents total number of lytic granules. The distance between the MTOC and the CS was

calculated after obtaining x and y coordinates of the MTOC centroid as well as those of the center of the YTS-target interface.

Intracellular Staining of Perforin and Granzyme B

Intracellular perforin and granzyme B levels were examined as previously described using FITC-perforin (BD) and FITC-granzyme B (BD) (20).

Lysosome Fractionation

Preparation of the crude lysosome fraction was performed as previously described (21). 40×10^6 YTS cells were resuspended with 500 μl of 0.25 M sucrose in 10mM Tris [pH 7.4] and homogenized with a dounce tissue homogenizer. The homogenate was spun at 600 × g for 5 min at 4 °C and the supernatant (postnuclear lysate; PNL) was collected and spun again at 12,000 × g for 10 min at 4 °C. The supernatant was then collected and $CaCl_2$ was added to the supernatant to a final concentration of 8 mM and mixed well. The mixture was then spun at 13,000 rpm for 15 min at 4 °C, and the supernatant was collected as the non-lysosomal fraction (NLF). Pellets were washed once with 150 mM KCl in 10 mM Tris [pH 7.4], resuspended with 80 μl of 150 mM KCl in 10 mM Tris [pH 7.4], and saved as the crude lysosomal fraction (CLF).

Cell Stimulation

In experiments involving cell surface receptor (NKG2D and 2B4) cross-linking, 15×10^6 NKL cells were prepared for each stimulation condition. Anti-NKG2D (R&D Systems) and anti-2B4 (clone C1.7) were added at a final concentration of 5 μg/ml to 150 μl of cell suspension and incubated together for 10 min on ice. Washed cells were then incubated with goat anti-mouse IgG $F(ab')_2$ (Cappel) at 37 °C for the indicated periods of time.

Statistical Analysis

Statistical analyses of % Lytic Units (Fig. 2B and 2C) were performed using a one-sample *t* test with a hypothetical value of 100. For statistical analyses of ‘percentage of incidences’ (bottom panels of Fig. 4B, 4C, 5B, and 5C), a proportion *z* test was performed. All other statistical analyses in this study were performed using a two-tailed Student’s t test.

RESULTS

HkRP3 interacts with DOCK8 and exists as an oligomer

Our prior mass spectrometry analysis aimed at identifying DOCK8-interacting partners detected WASP and talin as well as several additional proteins (8) including HkPR3, which is largely uncharacterized. According to an expressed sequence tag database (14), HkRP3 is preferentially expressed in hematopoietic cells and its expression in myeloid and monocytoid leukemic cell-lines as well as in endothelial cells was confirmed previously (15). However, its expression has not been examined in human NK cells. Therefore, we prepared two human NK cell lines, NKL and YTS, and primary human NK cells along with several other cell-lines, and examined HkRP3 expression at the protein level (Fig. 1A). HkRP3 expression was detected in all human NK cells as well as two other human

hematopoietic cell-lines (Jurkat T cells, and 721.221 B cells). Consistent with previous findings, we were not able to detect HkRP3 in 293T human embryonic kidney (HEK293T) or HeLa cells (15). Unexpectedly, we did not detect HkRP3 in the human myelogenous leukemia cell line K562.

Since HkRP3 was identified as a potential DOCK8-interacting protein, we first determined if they interacted by transfecting HEK293T cells with plasmids encoding FLAG.YFP or FLAG.YFP-DOCK8 along with EE-only or EE-tagged HkRP3. Consistent with our mass spectrometry results, we observed that HkRP3 co-immunoprecipitated with DOCK8 (Fig. 1B). Importantly, we were also able to confirm that endogenous DOCK8 and HkRP3 co-immunoprecipitated with each other in YTS cells (Fig. 1C).

Girdin was suggested to form an oligomer mediated by its N-terminal region (14, 22). The region responsible for oligomer formation is shared among the members of the Girdin family, suggesting that HkRP3 might also exist as an oligomer. To test this possibility, we first transfected HEK293T cells with plasmids encoding FLAG.YFP or FLAG.YFP-HkRP3 along with EE-only or EE-tagged HkRP3, and performed immunoprecipitation using anti-EE antibody. We consistently found that EE-tagged HkRP3 co-immunoprecipitated together with FLAG-tagged HkRP3 suggesting that it can interact with itself (Fig. 1D). We next tested whether the interaction was in fact mediated by the N-terminal region of HkRP3 by incubating either GST- or MBP-fused N-terminal HkRP3 proteins (Fig. 1E), and performing a GST pull-down assay (Fig. 1F). Significantly, the GST-fused first half of HkRP3 successfully pulled down the same region of HkRP3 fused with MBP. Although our findings do not represent the endogenous oligomerization state of HkRP3, these data indicate that HkRP3 minimally forms a homodimer similar to Girdin, and interacts with DOCK8.

HkRP3 mediates NK cell cytotoxicity

To determine whether HkRP3 is involved in NK cell cytotoxicity, we compared the cytotoxic activity of YTS cells after depletion of HkRP3 using two different siRNA oligonucleotide duplexes. Seventy-two hours after transfection, we examined natural cytotoxicity using the 721.221 B lymphoblastoid cell-line as tumor target cells (Fig. 2A). Consistent with our previous findings, DOCK8-depleted YTS cells showed less cytotoxicity compared to control siRNA-transfected cells (8). Surprisingly, both HkRP3-suppressed YTS cells showed strong defects in cytotoxic activity similar to that of DOCK8 (Fig. 2A, left and center). Relative cytotoxicity (Lytic Units) was also diminished in the HkRP3-depleted cells compared to that of the control group (Fig. 2A, right). We also observed a similar decrease in cytotoxicity toward 721.221 cells by both HkRP3-depleted NKL cells (Fig. 2B, left and center) and primary human NK clones (Fig. 2C, left and left center). We also examined cytotoxicity mediated by specific NK activating receptors (NKG2D or CD16) using P815 target cells in a reverse antibody dependent cellular cytotoxicity assay. Suppression of HkRP3 consistently decreased redirected cytotoxicity through CD16 (Fig. 2C, right center) and NKG2D (Fig. 2B, right and Fig. 2C, right). Taken together, these data identify HkRP3 as an essential regulator of NK cell-mediated cytotoxicity.

HkRP3 does not affect NK – Target cell conjugation

An early event during NK cell cytotoxicity is the binding of NK cells to target cells via integrin-mediated adhesion (3). We had previously shown that depletion of DOCK8 in NK cells resulted in a dramatic decrease in NK cell adhesion to target cells (8). To examine whether HkRP3 is involved in conjugate formation, we compared the adhesion of control transfected and HkRP3-suppressed YTS cells. YTS cells and 721.221 target cells pre-labeled with different fluorescent dyes were incubated together at 37°C, and the percentage of target-bound YTS cells was measured using flow cytometry. In contrast to DOCK8 depletion, which abrogated NK cell adhesion, HkRP3-suppressed YTS cells showed as efficient conjugate formation as control cells, suggesting that HkRP3 does not mediate conjugate formation of NK cells to target cells (Fig. 3A). In addition to increased affinity maturation via conformational change, integrins are also observed to accumulate at the center of the NK-target interface contributing to the formation of the CS (3). Therefore, we examined whether LFA-1 (CD11a:CD18) accumulation at the CS is normal in HkRP3-suppressed YTS cells. After 25 minutes of incubation of YTS cells with pre-labeled 721.221 cells, cells were fixed and stained for LFA-1 (Fig. 3B). Consistent with results from the conjugate formation assay, HkRP3-depleted YTS cells presented normal polarization of LFA-1 to the CS, similar to control YTS cells (Fig. 3B and 3C). However, as expected (8), most of the DOCK8-depleted YTS cells failed to polarize LFA-1 to the CS. Taken together, these data indicate that HkRP3 is an important regulator of NK cell-mediated cytotoxicity, but is not involved in the initial step of conjugate formation.

HkRP3 regulates convergence of lytic granules to the MTOC

Since loss of DOCK8 impacts MTOC polarization during NK cell killing, we next examined whether HkRP3 might regulate the polarization of lytic granules toward the CS. During NK cytotoxicity, two different steps of lytic granule polarization occur: 1) lytic granules rapidly accumulate around the MTOC as NK cells interact with target cells, and 2) the MTOC along with the converged lytic granules polarize toward the CS (3, 6). In most cases, a twenty-five minute incubation of control transfected YTS cells with 721.221 targets resulted in lytic granules (visualized by perforin stain, red) clustering around the MTOC (visualized by γ-tubulin stain, green) and polarization of the MTOC just behind the NK-target interface (Fig. 4A, left panel). In the case of DOCK8-depleted YTS cells, lytic granules converged around the MTOC, but the MTOC failed to polarize toward the CS in many conjugates, similar to what was observed previously (Fig. 4A, right panel) (7, 8). Surprisingly, in the case of HkRP3-suppressed YTS cells, not only did lytic granules fail to cluster around the MTOC, but the MTOC itself was also found to be distant from the CS (Fig. 4A, middle panel). To quantify the defective lytic granule clustering around the MTOC in HkRP3-depleted YTS cells, we measured the mean distance of lytic granules to the MTOC (see Materials and Methods for details) (Fig. 4B, top panel). Since we could not distinguish which individual conjugated YTS cells are successfully siRNA-depleted for our gene of interest due to limitations in antibody options, we placed the conjugated YTS cells into groups depending on the measured distances, and calculated the percentage of incidences (Fig. 4B, bottom panel). The mean lytic granule to MTOC distance of most conjugated control YTS cells fell within the range of 1-2 μm, and about a third of the conjugated cells displayed distances less than 1μm. In the case of both HkRP3- and DOCK8-depleted YTS cells, most of the mean

distances of lytic granules from the MTOC also fell within the range of 1-2 μm, similar to the control group. However, many of the HkRP3-depleted YTS cells presented mean granule to MTOC distances greater than 2 μm (Fig. 4B, bottom panel). Unexpectedly, many DOCK8-depleted YTS cells displayed very tight clustering of lytic granules toward the MTOC when conjugated, having the average distance of granule to MTOC less than 0.5 μm (Fig. 4A and 4B, bottom panel). We also measured the distance between the MTOC and the center of the CS to represent the degree of polarization of the MTOC to the CS (Fig. 4C, top panel). Almost half of the conjugated control YTS cells displayed MTOC distances close to the CS (0-5 μm) (Fig. 4C, bottom panel). In the case of both HkRP3- and DOCK8-depleted YTS cells, however, the MTOCs of many conjugated YTS cells were found to be distant from the CS (greater than 10 μm). These findings suggest that HkRP3 mediates lytic granule clustering to the MTOC as well as MTOC polarization to the CS. It further shows that DOCK8 depletion does not impact lytic granule clustering, and may in fact negatively regulate this step in the cytotoxic process.

Previously, it was shown that the clustering of lytic granules to the MTOC could be triggered by stimulation of NK activation receptors alone (6, 23). In the case of YTS cells, whereas stimulation of non-activating receptor CD45 does not cause convergence of lytic granules to the MTOC, stimulation through CD28 induces lytic granule clustering. To confirm whether HkRP3 regulates lytic granule clustering toward the MTOC, we stimulated YTS cells using anti-CD45- or anti-CD28-coated glass coverslips after depletion of HkRP3 or DOCK8 by siRNA. Following 25 minutes of incubation on coverslips coated with anti-CD28 antibodies, lytic granules from both control- and DOCK8-depleted YTS cells accumulated around the MTOC (Fig. 5A and 5B). Interestingly, lytic granules of many DOCK8-depleted YTS cells were again more tightly clustered to the MTOC (Fig. 5B, bottom panel). However, almost half of the HkRP3-depleted YTS cells had a more dispersed distribution of lytic granules (Fig. 5A and 5B). As expected, lytic granules did not cluster when the different groups of YTS cells were placed on anti-CD45 antibody-coated coverslips (Fig. 5C). These data suggest that HkRP3 mediates the clustering of lytic granules to the MTOC in stimulated NK cells.

HkRP3 mediates efficient transport of lytic granules to the MTOC

Clustering of lytic granules to the MTOC is dependent upon minus-end-directed movement of dynein motors along the MT network (6). Our findings in the previous section clearly suggest an important role of HkRP3 in convergence of lytic granules to the MTOC in stimulated YTS cells (Fig. 4 and Fig. 5). However, it does not provide detailed information on how MTOC-directed movement of lytic granules is affected when HkRP3 is depleted in NK cells. Does HkRP3-depletion in NK cells completely impair lytic granule transport to the MTOC, or does it affect the kinetics of the transport? To understand the observed phenotype of HkRP3-suppressed YTS cells in more detail, we assessed both accumulation of lytic granules to the MTOC and polarization of the MTOC toward the CS in control or HkRP3-depleted YTS cells conjugated with 721.221 target cells for various lengths of time (Fig. 6). For a more clear presentation of our data, we present averaged values of both the mean distance of lytic granules from the MTOC and the distance of the MTOC to the CS. In the case of control YTS cells, lytic granules were rapidly converged to the MTOC within 10

minutes of incubation with target cells (Fig. 6A and 6B). This corresponds to the previous finding that lytic granule clustering to the MTOC is an early and rapid event during NK cell activation (6). On the other hand, although the average distance of lytic granules from the MTOC gradually decreased throughout the time course, HkRP3-depleted YTS cells required 30 minutes to accumulate lytic granules to the MTOC (Fig. 6A and 6B). In addition, polarization of the MTOC to the CS was achieved later than lytic granule clustering in the case of control YTS cells, consistent with prior observations (Fig. 6A and 6C) (6). The mean distance between MTOC and the CS did not change significantly during the first 10 minutes of incubation. In later time points, however, most of the conjugated YTS cells displayed clear polarization of the MTOC toward the CS. Interestingly, in the case of HkRP3-depleted YTS cells, the average distance of the MTOC from the CS did not change throughout the time points examined (Fig. 6C). Since we could not completely deplete HkRP3 in YTS cells using siRNA transfection, the delayed transport of lytic granules to the MTOC might be due to the remaining activity of HkRP3. However, considering efficient suppression of HkRP3 (Fig. 2 and Fig. 3A), it is more likely that HkRP3 mediates processive transport of lytic granules toward the MTOC in activated NK cells. Taken together, these data suggest that HkRP3 regulates efficient transport of lytic granules toward the MTOC mediated by dynein motors.

HkRP3 directly interacts with microtubules through its C-terminal region

We next wanted to determine the localization of HkRP3 in NK cells interacting with target cells. We first confirmed the specificity of our purified rabbit polyclonal antibody toward HkRP3 using YTS cells treated with siRNA control or siHkRP3 (Supplemental Figure 1). We next examined where HkRP3 is localized in NK cells. Since we have observed defective clustering of lytic granules along the MT network when HkRP3 is absent (Fig. 4-6), we examined localization of HkRP3 along with MTs as well as perforin to identify lytic granules (Fig. 7A). We found strong staining of HkRP3 at the MTOC, as well as discrete puncta along MT filaments (Fig. 7A, top row). Although puncta of HkRP3 did not exactly co-localize with perforin, they were often detected adjacent to the perforin-stained lytic granule (Fig. 7A, second row, see inset). Considering limitations in the lateral resolution of standard confocal microscope used in this study (250 nm), further examination of endogenous localization of HkRP3 using super-resolution microscopy will be informative.

The finding that HkRP3 localized to the MTOC as well as along MTs was interesting, since every Girdin family protein contains a putative MT binding domain at its N-terminus (14). Although a similar localization pattern of Girdin has been reported (24), it has not yet been tested whether this homologous region actually binds to MTs. Furthermore, current knowledge suggests potential roles of Girdin family proteins in many different aspects of cell biology, but not in MT regulation or cargo transport along MTs. To determine whether HkRP3 directly interacts with MTs and to map the binding region, we performed a pelleting assay with *in vitro* polymerized MTs. Unexpectedly, within tested concentration of MTs, the N-terminal region of HkRP3 did not co-pellet with MTs (Supplemental Figure 2A). Since HkRP3 contains a unique region at the C-terminus, we next tested the possibility that the unique region is responsible for the direct interaction of HkRP3 with MTs. Although the C-terminal region of HkRP3 fused with glutathione S-transferase (GST) was not pelleted by

itself (Fig. 7B and 7C), it was co-pelleted when incubated with MTs, consistent with the idea that HkRP3 can interact with MTs and its punctate localization with MTs in cells. This was not due to non-specific interaction of GST with microtubules, since GST was not co-pelleted with MTs (Fig. 7C). Since HkRP3 directly interacts with MTs, it is possible that the impaired clustering of lytic granules in HkRP3-depleted YTS cells might be due to disruption of the MT network. However, when we examined the gross MT network in HkRP3-depleted YTS cells, we did not notice any conspicuous difference in HkRP3-suppressed YTS cells compared to control cells (Supplemental Figure 1B). These data demonstrate that HkRP3 directly interacts with MTs through its C-terminal unique region of HkRP3.

HkRP3 interacts with the Dynein-dynactin MT motor complex

Dynein is a ~1.2 MDa multi-subunit motor responsible for most of the minus end-directed transport of diverse cargoes along the MT network in eukaryotic cells (25). Dynein requires the dynactin complex for its cellular functions and exists as a dynein-dynactin complex (called dynein complex hereafter). Dynactin is considered an essential regulator of dynein by mediating the cellular localization of dynein, selection of its cargoes, and motor processivity. Significantly, the dynein complex is responsible for lytic granule clustering to the MTOC in NK and $CD8^+$ T cells (6, 26). Therefore, we speculated that HkRP3 might play a role(s) in regulating motor activity of the dynein complex in addition to its interaction with MTs. Importantly, we could confirm the endogenous interaction of HkRP3 with dynein intermediate chain (DIC), a component of the dynein motor, as well as with $p150^{Glued}$, which is a subunit of dynactin (Fig. 7D). The interactions of HkRP3 with these subunits might be due to, or dependent on, the interaction of HkRP3 with MTs, since the dynein complex also directly binds MTs. However, this was found not to be the case, as endogenous HkRP3 still co-precipitated with $p150^{Glued}$ in YTS cells even after nocodazole-induced destabilization of the MT network (Supplemental Figure 2B and Fig. 7D). As indicated above, HkRP3 contains an N-terminal region, two coiled-coil domains in the middle, and a unique C-terminal region (14, 15). To delineate the interacting region of HkRP3 with dynein motor complex subunits, we designed four non-overlapping fragments of HkRP3 fused with GST at the N-terminus (Fig. 7B). Then, using a GST pull-down assay, we mapped the interacting region of HkRP3 for each subunit of the dynein complex (Fig. 7E). DIC was mainly pulled down with the C-terminus of HkRP3. On the other hand, $p150^{Glued}$ was equally pulled down with both the C-terminus and the second half of the coiled-coil region. Next, we compared endogenous localization patterns of HkRP3 with that of DIC as well as $p150^{Glued}$. Both DIC and $p150^{Glued}$ appeared as puncta aligning with the MT network similar to HkRP3 (Fig. 7A, third and fourth row), but their staining patterns did not exactly overlap. Taken together, these data indicate that HkRP3 interacts with the dynein motor complex.

Inefficient transport of lytic granules toward the MTOC in the absence of HkRP3 in NK cells (Fig. 6) suggests that regulation of dynein motor activity might be impaired in HkRP3-depleted NK cells. As dynactin is known to be important for dynein processivity (25, 27), one possibility is that HkRP3 might be important for the stable interaction between dynein and dynactin. Based on the assumption that HkRP3 might mediate most of the transport

activity of the dynein complex in NK cells, we tested whether the interaction of the dynein motor with dynactin is affected in HkRP3-depleted NKLs following receptor stimulation. However, as shown in Supplemental Figure 3A, DIC immunoprecipitated similar levels of $p150^{Glued}$ throughout the time-course in both control and HkRP3-depleted NKL cells.

HkRP3 is found in the lytic granule fraction

Previously, Mentlik and colleagues reported that the dynein complex is constitutively localized at lytic granules of NK cells (6). Since HkRP3 not only interacts with dynein complex but also seems to regulate dynein complex-mediated lytic granule clustering along MTs, we questioned whether HkRP3 might also be localized at the lytic granules of NK cells. To determine the presence of HkRP3 in lytic granules, the lysosomal fraction was purified from YTS cells and evaluated by immunoblot (Fig. 7F). As can be seen, granzyme B, a major cytotoxic component of lytic granules, was detected only in the crude lysosomal fraction, whereas β-actin was abundant only in the non-lysosomal fraction. Interestingly, HkRP3 as well as the dynein complex subunits were also detected in the crude lysosomal fraction. Therefore, a fraction of HkRP3 co-purifies with lytic granules.

In non-immune cells, it was previously demonstrated that Rab-interacting lysosomal protein (RILP) recruits dynein complex to the late endosome/lysosome in association with Rab7 and oxysterol-binding protein-related protein 1L (ORP1L) (28, 29). Interestingly, Rab7 and RILP localized at lytic granules in T cells and YTS cells, and $CD8^+$ T cells over-expressing RILP displayed clustered lytic granules (26, 30, 31). It is possible that cytotoxic lymphocytes utilize HkRP3 as an additional regulator to recruit or dock the dynein complex to lytic granules. However, this was not the case, since localization of the dynein complex subunits did not seem to be affected when HkRP3 was depleted (Supplemental Figure 3B), nor did it affect the intracellular levels of perforin or granzyme B (Supplemental Figure 3C). Taken together, our data suggest that some proportion of HkRP3 constitutively associates with lytic granules in order to facilitate their efficient transport along MTs (Fig. 8).

DISCUSSION

Previously, it was demonstrated in endothelial cells that HkRP3 mediates ER stress response via its interaction with GRP78, so HkRP3 was named Gipie (GRP78-interacting protein induced by ER stress). However, considering its preferential expression in immune cells as well as its roles in NK cells that are similar to the general functions of Hook proteins, we prefer to keep its name as Hook-related protein 3 (HkRP3) as originally suggested by Simpson and colleagues (24). Here, we show that HkRP3, a novel DOCK8-interacting protein, is essential for NK cell mediated cytotoxicity through its effects on lytic granule transport and MTOC polarization. Interestingly, HkRP3 appeared as puncta coating the MT network and was found to accumulate at the MTOC. Using a biochemical approach, we show that the C-terminus of HkRP3, which is not shared among Girdin family proteins, directly interacts with MTs, while the N-terminus of HkRP3 is involved in oligomerization (minimally existing as a homodimer), similar to Girdin and Hook proteins (22, 32). Finally, we show that HkRP3 interacts with the dynein motor complex and it remains likely that this

interaction is required for lytic granule clustering. Taken together, these findings reveal a novel regulatory molecule, which is critical for NK cell cytotoxicity (Fig. 8).

Our findings support the idea that clustering of lytic granules to the MTOC is dynein-mediated and is an early and rapid event in NK cell cytotoxicity (6). Under two different experimental conditions, suppression of HkRP3 in YTS cells impaired rapid clustering of lytic granules, which is also observed when dynein motor function is inhibited in NK cells. In addition, the localization pattern of HkRP3 along MTs, the presence of HkRP3 in the lysosomal fraction, and interaction of HkRP3 with dynein motor complex all strongly suggest a close relationship of HkRP3 with the dynein motor complex in regulating the transport of lytic granules in NK cells. Our data indicate that the loss of HkRP3 did not affect the interaction of dynein with dynactin. Moreover, we observed no effect on the accumulation of either component in the lytic granule fraction in the absence of HkRP3. However, it remains possible, that while the dynein motor complex is tethered to its cargo, the processivity of the motor is not appropriately regulated in the absence of HkRP3. In fact, it was recently shown that the mammalian dynein-dynactin motor requires adaptor proteins to induce processive motility along MTs (33). Interestingly, the addition of Hook3 substantially increased the processivity of the dynein motor complex. Thus, while the dynein complex is constitutively localized at lytic granules in NK cells, it remains possible that the interaction of HkRP3 with the dynein motor complex would enhance its processive motor function leading to rapid lytic granule clustering to the MTOC. It is also important to note that Hook proteins have been suggested to mediate the tethering of different cargoes to the MT network (32, 34). They mediate this by binding to MTs using their highly conserved N-termini, and bind to their cargoes (organelles or proteins) via their more divergent C-termini. Similar domain organization of Hook proteins to that of CLIP-170, prototypic cytoplasmic linker protein, also supports potential roles of Hook proteins as another group of cytoplasmic MT linker proteins. Girdin family proteins also present similar domain organization to Hook proteins, although conservation between the two families of proteins is limited to the N-terminus which supposedly mediates interaction with MTs (14). Surprisingly, using a MT pelleting assay we were unable to detect any binding of the N-terminus to polymerized MTs. In contrast, we find that HkRP3 directly binds to MTs through its unique region located at the C-terminus, whereas the N-terminal ‘hook-related’ domain appears to promote HkRP3 homo-oligomerization. Therefore, HkRP3 is likely minimally a homodimer that acts as a MT-linker protein tethering lytic granules to the MT network either constitutively or in an activation-dependent manner (Fig. 8).

Understanding how HkRP3 cooperates with DOCK8 to mediate NK cell cytotoxicity will be another interesting topic for future studies. Although we mainly focused on elucidating cellular roles of HkRP3 in NK cell cytotoxicity in this study, observations from DOCK8-depleted YTS cells that we used as our positive control suggest clues as to how DOCK8 might be involved in the functions of HkRP3. We found that DOCK8-depleted YTS cells present very tight clustering of lytic granules, when they are stimulated. This unexpected observation suggests the possibility that DOCK8 might play regulatory roles in HkRP3-mediated lytic granule transport to the MTOC (Fig. 8). It will be interesting to examine whether the absence of DOCK8 affects the dynamic interaction of HkRP3 with MTs and the dynein complex, and thereby the kinetics of lytic granule transport to the MTOC.

Our data also suggest a role for HkRP3 in MTOC polarization following NK activation. In fact, while our time course experiments revealed that lytic granule convergence to the MTOC is delayed in the absence of HkRP3, MTOC polarization to the CS did not occur. A recent report has indicated that MTOC polarization to the synapse can occur independent of lytic granule clustering (6), thus HkRP3 is likely impacting both steps in this tightly-regulated process. Interestingly, the dynein motor complex has been shown to regulate MTOC polarization in T cells (35-37). It is also very important to note essential roles of CDC42 in MTOC polarization partly by regulating dynein motors (38-42). Considering the fact that DOCK8 is a GEF for CDC42, future studies focusing on roles of HkRP3 in MTOC polarization to the CS and its relationship with the dynein complex as well as with DOCK8 will provide a better understanding of the mechanism by which HkRP3 regulates MTOC polarization.

HkRP3 might also regulate the transport of lytic granules by coordinating not only motor activity of dynein but also that of kinesins, which are plus-end MT motors. Kinesin-1 has been suggested to mediate MTOC polarization of NK cells and final transport of lytic granules close to accumulated F-actin at the immune synapse of $CD8^+$ T cells (43, 44). Although roles of kinesin motors in regulating transport of lytic granules along MTs have not been examined in detail, it is logical to hypothesize that rapid movement of lytic granules along the MT network also requires kinesin-mediated anterograde transport. Rapid lytic granule clustering was demonstrated to occur in both cytolytic and non-cytolytic activation of NK cells, suggesting that the event might act as another checkpoint of NK cytotoxicity (6). When NK cells return to the resting state following activation, they require anterograde motor activity to disperse the lytic granules. Although we only examined the interaction of HkRP3 with dynein complex in this study, it is worthwhile to test whether HkRP3 also regulates kinesin activities. It is very interesting to note that Hok1, the fungus homologue of Hook proteins, was recently demonstrated to act as an adaptor for early endosome transport by coordinating activities of both dynein and kinesin-3 (45).

While revising our manuscript, HkRP3 (CCDC88B) was identified as a gene responsible for pathological inflammation via a genome-wide screen of ENU (*N*-ethyl-*N*-nitrosourea)-mutagenized mice (46). Loss of HkRP3 was found to induce resistance in an experimental cerebral malaria (ECM) model, which normally leads to severe inflammatory responses and lethality. Interestingly, HkRP3 was found to be important for maturation of activated T cells as well as production of inflammatory cytokines. Essential role(s) of HkRP3 in NK cell cytotoxicity demonstrated in our study provide another layer of explanation why HkRP3-mutant mice presented protection from ECM. However, it is not clear at this moment whether potential role(s) of HkRP3 in regulating dynein complex are also responsible for the observed T cell defects. The molecular mechanism by which HkRP3 mediates T cell maturation and its function requires further studies.

In addition to the points discussed above, several interesting questions need to be answered regarding HkRP3. Some of these include: 1) Does HkRP3 mediate transport of cargoes in immune cells other than lytic granules? 2) Does HkRP3 have any role in regulating the MT network (e.g. post-translational modification) to mediate cargo transport? Future studies focusing on HkRP3 will provide a better understanding of NK cell cytotoxicity and the

mechanistic regulation of MT motors involved in lytic granule clustering and MTOC polarization.

Supplementary Material

Refer to Web version on PubMed Central for supplementary material.

ACKNOWLEDGEMENTS

We specially thank Debra Evans for technical assistance in the immunofluorescence assay, helpful discussion, and critical reading of the manuscript. We are grateful to Joanna Kim for helpful suggestions on quantification of IF data. We also thank Cristina Correia for technical advice on purification of recombinant proteins for our *in vitro* assays. We are also appreciative of the members of the Billadeau laboratory for helpful discussions.

This work was supported by the Mayo Foundation and NCI grant R56-AI112538 to D.D.B. H.H was supported by the Mayo Graduate School. The Gene Analysis Core Shared Resource is supported in part by the Mayo Clinic Comprehensive Cancer Center Support Grant P30CA15083.

Abbreviations

CMAC	7-amino-4-chloromethylcoumarin
CS	cytotoxic synapse
DIC	dynein intermediate chain
GST	glutathione S-transferase
MBP	maltose-binding protein
MS	mass spectrometry
MT	microtubule
MTOC	microtubule organizing center
siRNA	small interfering RNA

REFERENCES

1. Vivier E, Tomasello E, Baratin M, Walzer T, Ugolini S. Functions of natural killer cells. Nat Immunol. 2008; 9:503–510. [PubMed: 18425107]
2. Gregoire C, Chasson L, Luci C, Tomasello E, Geissmann F, Vivier E, Walzer T. The trafficking of natural killer cells. Immunol Rev. 2007; 220:169–182. [PubMed: 17979846]
3. Ham H, Billadeau DD. Human immunodeficiency syndromes affecting human natural killer cell cytolytic activity. Front Immunol. 2014; 5:2. [PubMed: 24478771]
4. Orange JS. Formation and function of the lytic NK-cell immunological synapse. Nat Rev Immunol. 2008; 8:713–725. [PubMed: 19172692]
5. Wood SM, Ljunggren HG, Bryceson YT. Insights into NK cell biology from human genetics and disease associations. Cell Mol Life Sci. 2011; 68:3479–3493. [PubMed: 21874350]
6. Mentlik AN, Sanborn KB, Holzbaur EL, Orange JS. Rapid lytic granule convergence to the MTOC in natural killer cells is dependent on dynein but not cytolytic commitment. Mol Biol Cell. 2010; 21:2241–2256. [PubMed: 20444980]
7. Mizesko MC, Banerjee PP, Monaco-Shawver L, Mace EM, Bernal WE, Sawalle-Belohradsky J, Belohradsky BH, Heinz V, Freeman AF, Sullivan KE, Holland SM, Torgerson TR, Al-Herz W, Chou J, Hanson IC, Albert MH, Geha RS, Renner ED, Orange JS. Defective actin accumulation

impairs human natural killer cell function in patients with dedicator of cytokinesis 8 deficiency. J Allergy Clin Immunol. 2013; 131:840–848. [PubMed: 23380217]

8. Ham H, Guerrier S, Kim J, Schoon RA, Anderson EL, Hamann MJ, Lou Z, Billadeau DD. Dedicator of cytokinesis 8 interacts with talin and Wiskott-Aldrich syndrome protein to regulate NK cell cytotoxicity. J Immunol. 2013; 190:3661–3669. [PubMed: 23455509]
9. Engelhardt KR, McGhee S, Winkler S, Sassi A, Woellner C, Lopez-Herrera G, Chen A, Kim HS, Lloret MG, Schulze I, Ehl S, Thiel J, Pfeifer D, Veelken H, Niehues T, Siepermann K, Weinspach S, Reisli I, Keles S, Genel F, Kutukculer N, Camcioglu Y, Somer A, Karakoc-Aydiner E, Barlan I, Gennery A, Metin A, Degerliyurt A, Pietrogrande MC, Yeganeh M, Baz Z, Al-Tamemi S, Klein C, Puck JM, Holland SM, McCabe ER, Grimbacher B, Chatila TA. Large deletions and point mutations involving the dedicator of cytokinesis 8 (DOCK8) in the autosomal-recessive form of hyper-IgE syndrome. J Allergy Clin Immunol. 2009; 124:1289–1302. e1284. [PubMed: 20004785]
10. Su HC, Jing H, Zhang Q. DOCK8 deficiency. Ann N Y Acad Sci. 2011; 1246:26–33. [PubMed: 22236427]
11. Zhang Q, Davis JC, Lamborn IT, Freeman AF, Jing H, Favreau AJ, Matthews HF, Davis J, Turner ML, Uzel G, Holland SM, Su HC. Combined immunodeficiency associated with DOCK8 mutations. N Engl J Med. 2009; 361:2046–2055. [PubMed: 19776401]
12. Harada Y, Tanaka Y, Terasawa M, Pieczyk M, Habiro K, Katakai T, Hanawa-Suetsugu K, Kukimoto-Niino M, Nishizaki T, Shirouzu M, Duan X, Uruno T, Nishikimi A, Sanematsu F, Yokoyama S, Stein JV, Kinashi T, Fukui Y. DOCK8 is a Cdc42 activator critical for interstitial dendritic cell migration during immune responses. Blood. 2012
13. Randall KL, Chan SS, Ma CS, Fung I, Mei Y, Yabas M, Tan A, Arkwright PD, Al Suwairi W, Lugo Reyes SO, Yamazaki-Nakashimada MA, Garcia-Cruz Mde L, Smart JM, Picard C, Okada S, Jouanguy E, Casanova JL, Lambe T, Cornall RJ, Russell S, Oliaro J, Tangye SG, Bertram EM, Goodnow CC. DOCK8 deficiency impairs CD8 T cell survival and function in humans and mice. J Exp Med. 2011; 208:2305–2320. [PubMed: 22006977]
14. Enomoto A, Ping J, Takahashi M. Girdin, a novel actin-binding protein, and its family of proteins possess versatile functions in the Akt and Wnt signaling pathways. Ann N Y Acad Sci. 2006; 1086:169–184. [PubMed: 17185515]
15. Matsushita E, Asai N, Enomoto A, Kawamoto Y, Kato T, Mii S, Maeda K, Shibata R, Hattori S, Hagikura M, Takahashi K, Sokabe M, Murakumo Y, Murohara T, Takahashi M. Protective role of Gipie, a Girdin family protein, in endoplasmic reticulum stress responses in endothelial cells. Mol Biol Cell. 2011; 22:736–747. [PubMed: 21289099]
16. Windebank KP, Abraham RT, Powis G, Olsen RA, Barna TJ, Leibson PJ. Signal transduction during human natural killer cell activation: inositol phosphate generation and regulation by cyclic AMP. J Immunol. 1988; 141:3951–3957. [PubMed: 2846696]
17. Banerjee PP, Pandey R, Zheng R, Suhoski MM, Monaco-Shawver L, Orange JS. Cdc42-interacting protein-4 functionally links actin and microtubule networks at the cytolytic NK cell immunological synapse. J Exp Med. 2007; 204:2305–2320. [PubMed: 17785506]
18. Maasho K, Marusina A, Reynolds NM, Coligan JE, Borrego F. Efficient gene transfer into the human natural killer cell line, NKL, using the Amaxa nucleofection system. J Immunol Methods. 2004; 284:133–140. [PubMed: 14736423]
19. Gomez TS, Hamann MJ, McCarney S, Savoy DN, Lubking CM, Heldebrant MP, Labno CM, McKean DJ, McNiven MA, Burkhardt JK, Billadeau DD. Dynamin 2 regulates T cell activation by controlling actin polymerization at the immunological synapse. Nat Immunol. 2005; 6:261–270. [PubMed: 15696170]
20. Piotrowski JT, Gomez TS, Schoon RA, Mangalam AK, Billadeau DD. WASH knockout T cells demonstrate defective receptor trafficking, proliferation, and effector function. Mol Cell Biol. 2013; 33:958–973. [PubMed: 23275443]
21. Schenkman JB, Cinti DL. Preparation of microsomes with calcium. Methods Enzymol. 1978; 52:83–89. [PubMed: 672658]
22. Enomoto A, Murakami H, Asai N, Morone N, Watanabe T, Kawai K, Murakumo Y, Usukura J, Kaibuchi K, Takahashi M. Akt/PKB regulates actin organization and cell motility via Girdin/APE. Dev Cell. 2005; 9:389–402. [PubMed: 16139227]

23. James AM, Hsu HT, Dongre P, Uzel G, Mace EM, Banerjee PP, Orange JS. Rapid activation receptor- or IL-2-induced lytic granule convergence in human natural killer cells requires Src, but not downstream signaling. Blood. 2013; 121:2627–2637. [PubMed: 23380740]
24. Simpson F, Martin S, Evans TM, Kerr M, James DE, Parton RG, Teasdale RD, Wicking C. A novel hook-related protein family and the characterization of hook-related protein 1. Traffic. 2005; 6:442–458. [PubMed: 15882442]
25. Kardon JR, Vale RD. Regulators of the cytoplasmic dynein motor. Nat Rev Mol Cell Biol. 2009; 10:854–865. [PubMed: 19935668]
26. Daniele T, Hackmann Y, Ritter AT, Wenham M, Booth S, Bossi G, Schintler M, Auer-Grumbach M, Griffiths GM. A role for Rab7 in the movement of secretory granules in cytotoxic T lymphocytes. Traffic. 2011; 12:902–911. [PubMed: 21438969]
27. King SJ, Schroer TA. Dynactin increases the processivity of the cytoplasmic dynein motor. Nat Cell Biol. 2000; 2:20–24. [PubMed: 10620802]
28. Johansson M, Rocha N, Zwart W, Jordens I, Janssen L, Kuijl C, Olkkonen VM, Neefjes J. Activation of endosomal dynein motors by stepwise assembly of Rab7-RILP-p150Glued, ORP1L, and the receptor betalll spectrin. J Cell Biol. 2007; 176:459–471. [PubMed: 17283181]
29. Jordens I, Fernandez-Borja M, Marsman M, Dusseljee S, Janssen L, Calafat J, Janssen H, Wubbolts R, Neefjes J. The Rab7 effector protein RILP controls lysosomal transport by inducing the recruitment of dynein-dynactin motors. Curr Biol. 2001; 11:1680–1685. [PubMed: 11696325]
30. Casey TM, Meade JL, Hewitt EW. Organelle proteomics: identification of the exocytic machinery associated with the natural killer cell secretory lysosome. Mol Cell Proteomics. 2007; 6:767–780. [PubMed: 17272266]
31. Stinchcombe JC, Majorovits E, Bossi G, Fuller S, Griffiths GM. Centrosome polarization delivers secretory granules to the immunological synapse. Nature. 2006; 443:462–465. [PubMed: 17006514]
32. Walenta JH, Didier AJ, Liu X, Kramer H. The Golgi-associated hook3 protein is a member of a novel family of microtubule-binding proteins. J Cell Biol. 2001; 152:923–934. [PubMed: 11238449]
33. McKenney RJ, Huynh W, Tanenbaum ME, Bhabha G, Vale RD. Activation of cytoplasmic dynein motility by dynactin-cargo adapter complexes. Science. 2014; 345:337–341. [PubMed: 25035494]
34. Maldonado-Baez L, Cole NB, Kramer H, Donaldson JG. Microtubule-dependent endosomal sorting of clathrin-independent cargo by Hook1. J Cell Biol. 2013; 201:233–247. [PubMed: 23589492]
35. Combs J, Kim SJ, Tan S, Ligon LA, Holzbaur EL, Kuhn J, Poenie M. Recruitment of dynein to the Jurkat immunological synapse. Proc Natl Acad Sci U S A. 2006; 103:14883–14888. [PubMed: 16990435]
36. Liu X, Kapoor TM, Chen JK, Huse M. Diacylglycerol promotes centrosome polarization in T cells via reciprocal localization of dynein and myosin II. Proc Natl Acad Sci U S A. 2013; 110:11976–11981. [PubMed: 23818610]
37. Yi J, Wu X, Chung AH, Chen JK, Kapoor TM, Hammer JA. Centrosome repositioning in T cells is biphasic and driven by microtubule end-on capture-shrinkage. J Cell Biol. 2013; 202:779–792. [PubMed: 23979719]
38. Etienne-Manneville S, Hall A. Integrin-mediated activation of Cdc42 controls cell polarity in migrating astrocytes through PKCzeta. Cell. 2001; 106:489–498. [PubMed: 11525734]
39. Gomes ER, Jani S, Gundersen GG. Nuclear movement regulated by Cdc42, MRCK, myosin, and actin flow establishes MTOC polarization in migrating cells. Cell. 2005; 121:451–463. [PubMed: 15882626]
40. Palazzo AF, Joseph HL, Chen YJ, Dujardin DL, Alberts AS, Pfister KK, Vallee RB, Gundersen GG. Cdc42, dynein, and dynactin regulate MTOC reorientation independent of Rho-regulated microtubule stabilization. Curr Biol. 2001; 11:1536–1541. [PubMed: 11591323]
41. Schmoranzer J, Fawcett JP, Segura M, Tan S, Vallee RB, Pawson T, Gundersen GG. Par3 and dynein associate to regulate local microtubule dynamics and centrosome orientation during migration. Curr Biol. 2009; 19:1065–1074. [PubMed: 19540120]

42. Yuseff MI, Reversat A, Lankar D, Diaz J, Fanget I, Pierobon P, Randrian V, Larochette N, Vascotto F, Desdouets C, Jauffred B, Bellaiche Y, Gasman S, Darchen F, Desnos C, Lennon-Dumenil AM. Polarized secretion of lysosomes at the B cell synapse couples antigen extraction to processing and presentation. Immunity. 2011; 35:361–374. [PubMed: 21820334]

43. Tuli A, Thiery J, James AM, Michelet X, Sharma M, Garg S, Sanborn KB, Orange JS, Lieberman J, Brenner MB. Arf-like GTPase Arl8b regulates lytic granule polarization and natural killer cell-mediated cytotoxicity. Mol Biol Cell. 2013

44. Kurowska M, Goudin N, Nehme NT, Court M, Garin J, Fischer A, de Saint Basile G, Menasche G. Terminal transport of lytic granules to the immune synapse is mediated by the kinesin-1/Slp3/Rab27a complex. Blood. 2012; 119:3879–3889. [PubMed: 22308290]

45. Bielska E, Schuster M, Roger Y, Berepiki A, Soanes DM, Talbot NJ, Steinberg G. Hook is an adapter that coordinates kinesin-3 and dynein cargo attachment on early endosomes. J Cell Biol. 2014; 204:989–1007. [PubMed: 24637326]

46. Kennedy JM, Fodil N, Torre S, Bongfen SE, Olivier JF, Leung V, Langlais D, Meunier C, Berghout J, Langat P, Schwartzentruber J, Majewski J, Lathrop M, Vidal SM, Gros P. CCDC88B is a novel regulator of maturation and effector functions of T cells during pathological inflammation. J Exp Med. 2014; 211:2519–2535. [PubMed: 25403443]

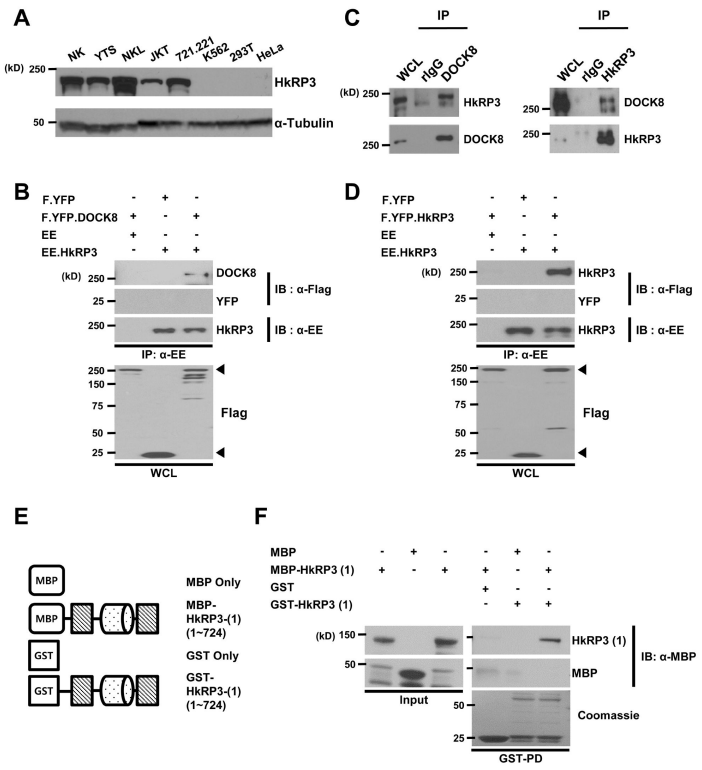

Figure 1.

HkRP3 is expressed in NK cells, interacts with DOCK8, and forms an oligomer. (A) Immunoblot for HkRP3 in whole cell lysates from a primary human NK clone, human NK cell-lines (NKL and YTS), and other cell-lines (top). Immunoblot for α-tubulin was shown as a loading control (bottom). JKT, Jurkat T cells; 293T, 293T human embryonic kidney cells. (B) HEK 293T cells were transfected with the indicated plasmids. Two days post-transfection, cell lysate was immunoprecipitated with anti-EE, and examined for DOCK8 (FLAG). Arrowheads denote bands of FLAG-tagged proteins from whole cell lysates (WCL). (C) Immunoblot analysis of whole cell lysates with anti-DOCK8, or anti-HkRP3 immunoprecipitates (IP) derived from YTS cells. IP with rabbit IgG (rIgG) was used as a negative control. (D) HEK 293T cells were transfected with the indicated plasmids. Two days post-transfection, cell lysate was immunoprecipitated with anti-EE, and examined for HkRP3 (FLAG). Arrowheads denote bands of FLAG-tagged proteins from whole cell lysates (WCL). (E) Schematic representation of HkRP3 fragments used for GST pull-down assays in (F). Cylinder shape represents coiled-coil region. (F) MBP or MBP-HkRP3 (1) (aa 1-724) were pulled down by GST or GST- HkRP3 (1) (aa 1-724) as denoted above the lanes, and examined for MBP or HkRP3 by immunoblot (top and middle). Coomassie blue staining shows GST fusion proteins used in the pull-down assay (bottom). Data shown are representative of three independent experiments.

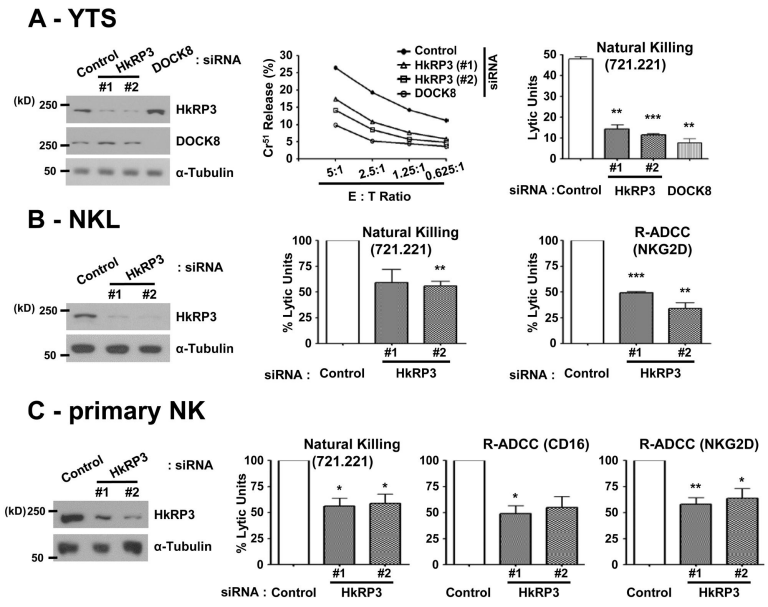

Figure 2.

HkRP3 mediates NK cell cytotoxicity. (A-C) The indicated NK cell types were nucleofected with control, HkRP3 or DOCK8 siRNAs. 72 hours post nucleofection, cell lysates were prepared and immunoblotted with the indicated antibodies (left panels). (A) Nucleofected YTS cells were incubated with ^{51}Cr-labeled 721.221 cells and the percent specific release was measured over the indicated effector:target (E:T) ratios (center). Cytotoxic activity of control, HkRP3- or DOCK8-depleted YTS cells was assessed and expressed as Lytic Units (LU) (right). Data shown are representative (left and center) or average (right) of three independent experiments. (B) LU values of NKL cells transfected with the indicated siRNA oligos against 721.221 target cells (center) or P815 target cells coated with anti-NKG2D (right) were calculated and presented as a percentage of LU values of the control group. Data shown are representative (left) or an average of three independent experiments. (C) LU values of primary human NK clones transfected with the indicated siRNA oligos against 721.221 (left center) or P815 target cells coated with anti-CD16 (right center) or anti-NKG2D (right) were calculated and presented as a percentage of LU values of the control group. Data shown are representative (left) or an average of three (721.221 and CD16) and four (NKG2D) independent experiments. Error bars indicate SEM. *$P < 0.05$, ** $P < 0.01$, and ***$P < 0.005$ compared with control group.

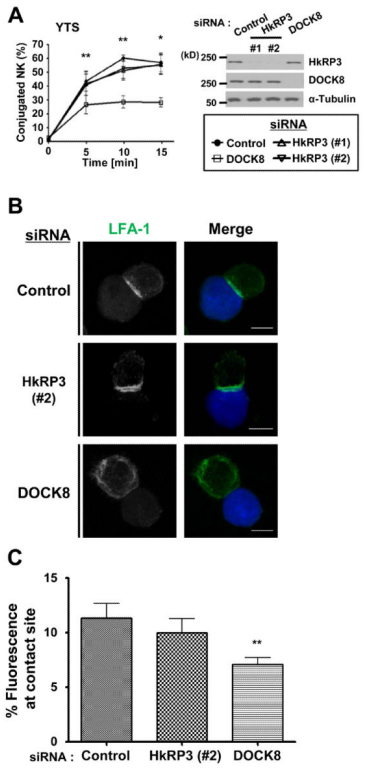

Figure 3.

HkRP3 does not modulate NK conjugate formation. (A) YTS cells were nucleofected with the indicated siRNAs. 72 h post-nucleofection, YTS cells were stained with CellTracker Violet and then incubated with CFSE-labeled 721.221 cells for the indicated times at 37 °C. The percentage of conjugated YTS cells was assessed using two-color flow cytometry and calculated based on simultaneous emission of both violet and green fluorescence. Presented data are the average of four independent experiments performed in duplicate or triplicate. Error bars indicate SEM. $*P < 0.05$, and $**P < 0.01$ compared with control group. (B and C) YTS cells were transfected with the indicated siRNA oligos. At 72 h, these cells were conjugated with CMAC-stained 721.221 target cells (blue), incubated for a total of 25 min at 37 °C, and fixed for immunofluorescence staining. (B) Representative images from three independent experiments (LFA-1: green). Bars, 10 μm. (C) Scoring of LFA-1 polarization to the YTS-721.221 interface (see Materials and Methods for details). Data shown are collected from three independent experiments. Error bars indicate SEM. $**P < 0.01$ compared with control group.

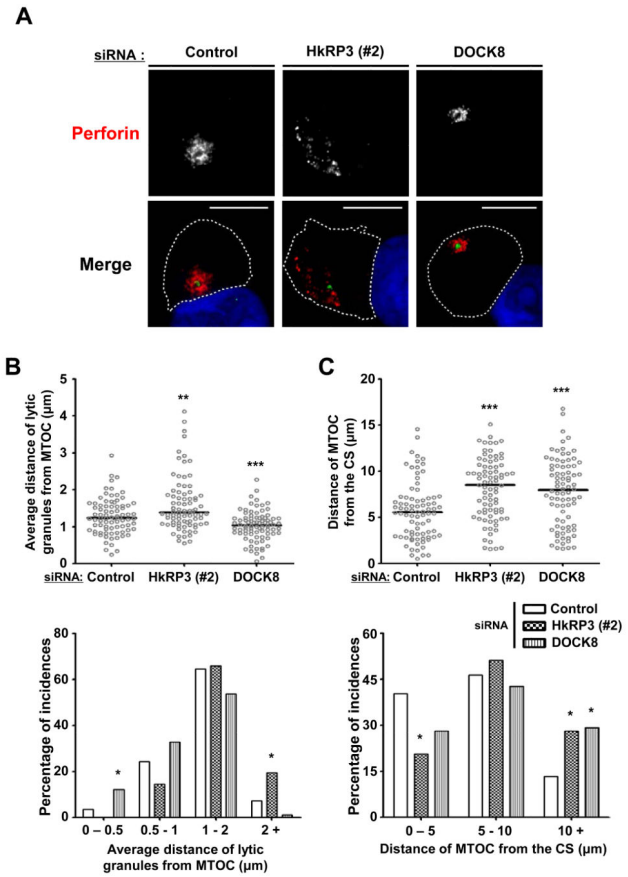

Figure 4.

HkRP3 regulates lytic granule clustering to the MTOC as well as MTOC polarization to the CS. (A-C) YTS cells were transfected with the indicated siRNA oligos. At 72 h, these cells were conjugated with CMAC-stained 721.221 target cells (blue), incubated for a total of 25 min at 37 °C, and fixed for immunofluorescence staining. (A) Representative images from five independent experiments (perforin: red, and γ-tubulin: green). Bars, 10 μm. (B) Average distances of lytic granules from the MTOC were measured from 82 conjugated YTS cells per each experimental group (15-20 conjugated YTS cells per experiment; 5 independent experiments; see Materials and Methods for details). Top panel: scatter plot of mean distances of lytic granules from the MTOC. Bar, median. Bottom panel: percentage of incidences based on mean distances of lytic granules from the MTOC. (C) Distances of the MTOC from the center of the CS were measured from 82 conjugated YTS cells per each experimental group (15-20 conjugated YTS cells per experiment; 5 independent experiments; see Materials and Methods for details). Top panel: scatter plot of distances of the MTOC from the center of the CS. Bar, median. Bottom panel: percentage of incidences based on distances of the MTOC from the center of the CS. **P* < 0.05, ***P* < 0.01, and ****P* < 0.005 compared with control group.

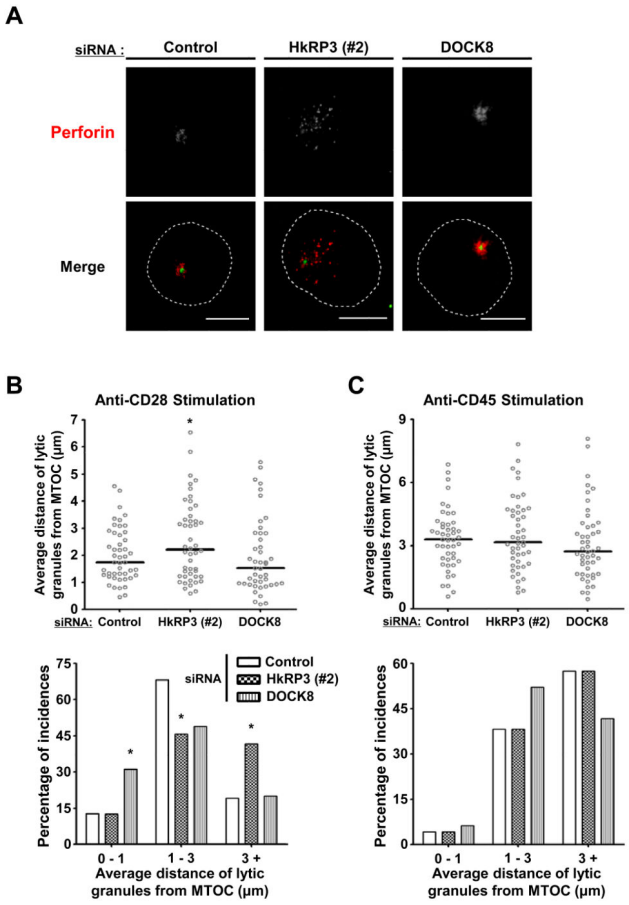

Figure 5.

HkRP3 mediates lytic granule clustering to the MTOC after stimulation with anti-CD28. (A-C) At 72 h after siRNA transfection into YTS cells as indicated, cells were placed on anti-CD28-coated (A and B) or anti-CD45-coated (C) coverslips, incubated for 25 min at 37 °C, and fixed for immunofluorescence staining. (A) Representative images from three independent experiments with anti-CD28 stimulation (perforin: red, and γ-tubulin: green). Bars, 10 μm. (B and C) Average distances of lytic granules from the MTOC were measured from 45-48 YTS cells per each experimental group (15-20 conjugated YTS cells per experiment; 3 independent experiments; see Materials and Methods for details). Top panels: Scatter plot of mean distances of lytic granules from the MTOC. Bar, median. Bottom panels: percentage of incidences based on mean distances of lytic granules from the MTOC. *$P < 0.05$ compared with control group.

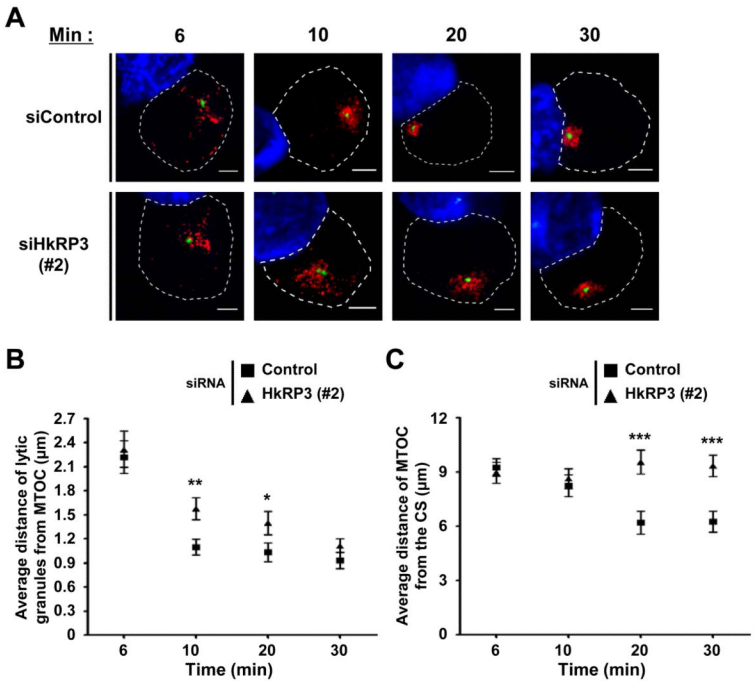

Figure 6.

HkRP3 regulates efficient transport of lytic granules to the MTOC. (A-C) 72 h after siRNA nucleofection, YTS cells were conjugated with CMAC-stained 721.221 target cells (blue), incubated for the indicated times at 37 °C, and fixed for immunofluorescence staining. (A) Representative images from three independent experiments (perforin: red, and γ-tubulin: green). Bars, 5 μm. (B) Average distances of lytic granules from the MTOC were measured for 30-35 conjugated YTS cells per each experimental group (10-12 conjugates per experiment; 3 independent experiments), and averaged. (C) Distances of the MTOC from the center of the CS were measured for 30-35 conjugated YTS cells per each time point (10-12 conjugates per experiment; 3 independent experiments), and averaged. Error bars indicate SEM. *$P < 0.05$, ** $P < 0.01$, and ***$P < 0.005$ compared with control group.

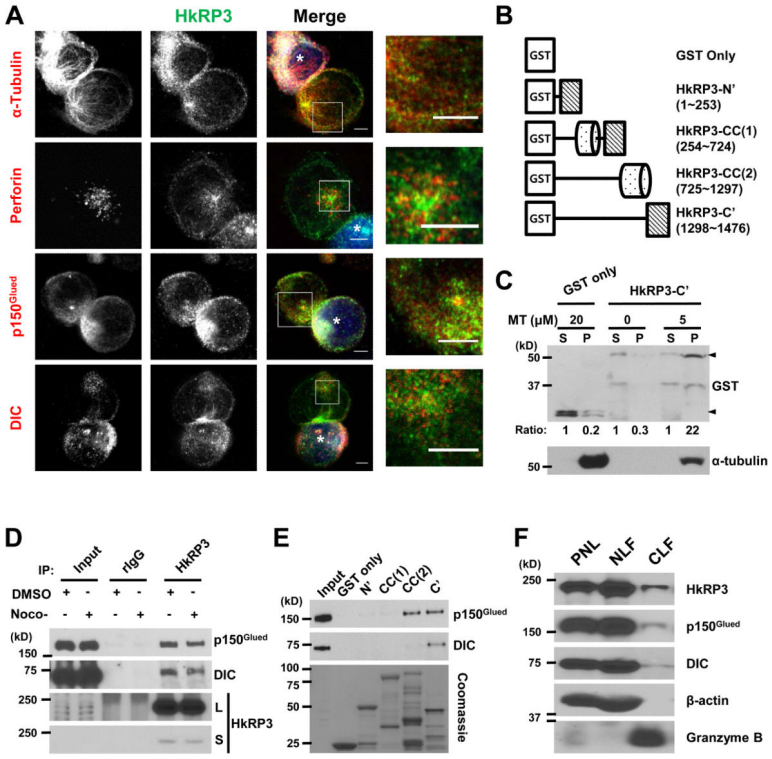

Figure 7.

HkRP3 exists in lytic granules, binds microtubules and interacts with the dynein motor complex. (A) YTS cells were conjugated with CMAC-stained 721.221 target cells (blue, marked with white asterisk), incubated for a total of 25 min at 37 °C, and fixed for immunofluorescence staining with the indicated antibodies. Images are representative of three independent experiments. Bars, 5 μm. (B) Schematic representation of HkRP3 fragments used for MT co-pelleting assay (C) and GST pull-down assays (E). Cylinder shape represents coiled-coil region. (C) Microtubule co-pelleting assay. 0.5μM of either GST or GST-HkRP3-C' was incubated with MTs of indicated concentrations. After centrifugation, supernatants (S) and pellets (P) were collected and examined for α-tubulin and GST by immunoblot. Arrowheads denote GST-fusion proteins. The numbers beneath the GST blot provide a densitometric ratio of each signal to signal from the supernatant fraction within the same sample group. Data shown are representative of three independent experiments. (D) YTS cells were treated with 10 μM nocodazole or the same volume of DMSO for 1 h at 37 °C, and washed. Some cells were fixed for immunofluorescence staining for α-tubulin to confirm disruption of the microtubule network (Supplemental Figure 2B). The remaining cells were lysed and immunoprecipitated using anti-HkRP3. IP with rabbit IgG (rIgG) was used as a negative control. Whole cell lysates and immunoprecipitates were examined for HkRP3, $p150^{Glued}$, and dynein intermediate chain (DIC). Data shown are representative of five independent experiments. L, long exposure; S, short exposure. (E) Lysates from YTS cells were pulled down by GST or GST-HkRP3 fragments and examined for $p150^{Glued}$, and dynein intermediate chain (DIC) by immunoblot. Coomassie blue staining shows GST fusion proteins used in the pull-down assay (bottom). Data shown are representative of three independent experiments. (F)

Postnuclear lysate (PNL), non-lysosomal fraction (NLF), and crude lysosomal fraction (CLF) were prepared from YTS cells, and examined for HkRP3, $p150^{Glued}$, DIC, β-actin, and granzyme B by immunoblot. Data shown are representative of three independent experiments.

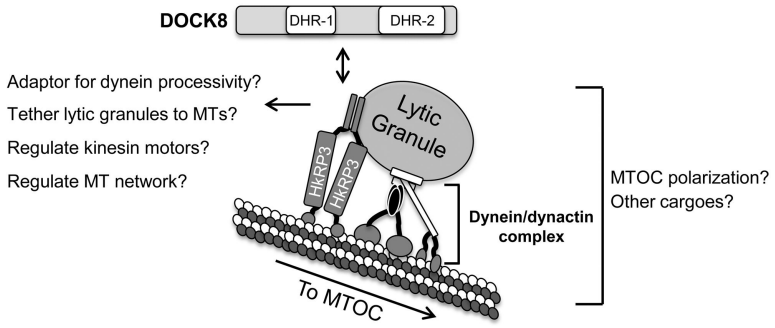

Figure 8.

Hypothetical model for how HkRP3 mediates lytic granule transport to the MTOC. See text for details.